

Article

Preparation and Characterization of Modified ZrO₂/SiO₂/Silicone-Modified Acrylic Emulsion Superhydrophobic Coating

Jixin Ben ¹, Peipei Wu ², Yancheng Wang ¹, Jie Liu ^{2,*} and Yali Luo ²

¹ College of 2011, Nanjing Tech University, Nanjing 211800, China

² College of Materials Science and Engineering, Nanjing Tech University, Nanjing 211800, China

* Correspondence: liujiecailiao@njtech.edu.cn

Abstract: Superhydrophobic coatings have increasingly become the focal point of research due to their distinctive properties like water resistance, wear resistance, and acid-base resilience. In pursuit of maximizing their efficiency, research has primarily revolved around refining the fabrication process and the composition of emulsion/nanoparticle coatings. We innovatively devised a superhydrophobic coating by employing a spraying technique. This involved integrating a γ-Methacryloyloxypropyltrimethoxysilane (KH570)-modified ZrO₂/SiO₂/silicone-modified acrylic emulsion. A comprehensive evaluation of this coating was undertaken using analytical instruments such as Fourier transform infrared spectroscopy (FTIR), X-ray diffraction (XRD), scanning electron microscopy (SEM), energy dispersive spectroscopy (EDS), and confocal laser scanning microscopy (CLSM). The coating demonstrated exceptional performance across a range of tests, including wear, immersion, and anti-icing cleaning, showcasing notable wear resistance, sodium chloride corrosion resistance, self-cleaning efficiency, and thermal stability. In particular, one coating exhibited super-hydrophobic properties, with a high contact angle of 158.5 degrees and an impressively low rolling angle of 1.85 degrees. This remarkable combination of properties is attributed to the judicious selection of components, which significantly reinforced the mechanical strength of the coating. These enhancements make it highly suitable for industrial applications where self-cleaning, anti-icing, and anti-contamination capabilities are critical.



Citation: Ben, J.; Wu, P.; Wang, Y.; Liu, J.; Luo, Y. Preparation and Characterization of Modified ZrO₂/SiO₂/Silicone-Modified Acrylic Emulsion Superhydrophobic Coating. *Materials* **2023**, *16*, 7621.

<https://doi.org/10.3390/ma16247621>

Academic Editor: Sergei A. Kulnich

Received: 31 October 2023

Revised: 9 December 2023

Accepted: 11 December 2023

Published: 13 December 2023



Copyright: © 2023 by the authors. Licensee MDPI, Basel, Switzerland. This article is an open access article distributed under the terms and conditions of the Creative Commons Attribution (CC BY) license (<https://creativecommons.org/licenses/by/4.0/>).

1. Introduction

Superhydrophobic coatings are notable for their ability to achieve contact angles greater than 150° for droplets, while simultaneously maintaining a rolling angle below 5° [1]. Such characteristics render them invaluable in various applications, including oil-water separation [2,3], anti-icing mechanisms [4,5], chemical analysis [6,7], antimicrobial medical solutions [8], and solar panels [9]. These coatings are engineered by combining emulsion surfaces with nanoparticle overlays, ensuring both optimal surface roughness for air entrapment and minimal surface activation energy to repel water molecules.

Different methodologies, such as etching [10–12], templating [13–15], sol-gel [16–18], spray coating [19–21], spin coating [22–24], and electrospinning [25–27], have been investigated to develop superhydrophobic coatings. Among the materials employed, nanoparticles are favored for their inherent hardness and distinct micro-nanostructures, which have proven pivotal in generating superhydrophobic surfaces. In terms of industrial production, it is imperative that these coatings exhibit both robust adhesion to substrates and remarkable mechanical resilience. To ensure these features, silicone-modified acrylic emulsion are utilized as binders, effectively binding the nanoparticles to the substrate. This structure is known as the “substrate/binder/superhydrophobic nanoparticle” system.

However, there remain challenges to address, especially when considering applications like medical implants, seawater desalination, and cable transmission. These applications demand coatings that resist acids and bases, exhibit anti-icing efficiency, and maintain self-cleaning attributes. To address these challenges, the researchers prepared superhydrophobic coatings with excellent acid and alkali resistance, ice resistance and self-cleaning capability by adding nanoparticles such as SiO_2 [28,29], TiO_2 [30,31], ZnO [32,33], Fe_3O_4 [34,35] and Al_2O_3 [36,37] to various polymer matrices. Yang et al. [38] synthesized a superhydrophobic coating by combining ZrO_2 with polydimethylsiloxane (PDMS). This PDMS- ZrO_2 composite coating exhibited outstanding corrosion resistance. Celik et al. [39] developed a superhydrophobic coating with remarkable corrosion resistance and self-cleaning properties. They achieved this by the ball milling process inducing a reaction between dodecyltrichlorosilane's trichloroalkylsilane and hydrophilic silica nanoparticles, leading to chemical grafting. Superhydrophobic coatings have been successfully utilized in anti-icing applications. Specifically, Qi et al. [40] employed an etching technique to evenly distribute SAN particles, dissolved by ASA resin, within a THF and EtOH solvent mixture to fabricate a hydrophobic surface. Notably, at a chilling ambient temperature of -10 degrees Celsius, the time taken for water droplets to crystallize on this coated surface was significantly prolonged to 63 min, indicating superior anti-icing efficacy.

To prepare wear-resistant superhydrophobic coatings using fillers in resin, two main methods are employed. The first approach involves directly incorporating fillers into the resin, thereby creating a coarse surface texture. Here, the filler becomes entirely wetted by the resin. This results in the development of a surface roughness predominantly via particles, while the resin contributes to the reduced surface energy. This synergy enables super hydrophobicity. A key advantage of this technique is that the introduction of ample fillers ensures a uniform rough structure both internally and externally. Coupled with the intrinsic hydrophobic nature of the resin, this ensures that the coating retains its superhydrophobic property until completely worn out. This method is presently the dominant means of achieving super hydrophobicity using fillers. However, its downside is that the film's overall strength diminishes due to the extensive filler content, leading to hydrophobicity degradation when sanded. Furthermore, it exhibits poor resistance to impacts and abrasions, causing the coating to detach easily from the substrate.

The alternative approach is to use the “adhesive + particle” [41,42] method, utilizing potent adhesives like epoxy resin and water-based polyurethane to bind hard hydrophobic particles directly onto the coating, providing friction resistance in a robust manner. In this scenario, the particles serve dual functions: bestowing reduced surface energy and imparting surface roughness. The superhydrophobic coatings derived via this method exhibit enhanced hydrophobicity and, given the minimal particle incorporation within adhesive, have superior post-film formation strength.

Interestingly, there seems to be an oversight in current research regarding the potential of ZrO_2 nanoparticles. Furthermore, many current methods demand intricate steps, high-tech equipment, and can be operationally challenging, especially when contrasted with the industry-preferred spray coating technique. To bridge this gap, our research introduces a novel coating formulation. Some silicone-modified acrylic emulsion was pre-introduced into the ethanol suspension. By incorporating SiO_2 particles and ZrO_2 nanoparticles modified with the silane coupling agent KH-570, into the ethanol mixture, we achieved diverse composite coatings. With the strategic use of silicone-modified acrylic emulsion and selected nanoparticles, we developed a superhydrophobic coating via the spray coating technique. The rigorous assessment addressed wear resistance, adaptability in acidic and alkaline conditions, durability against sodium chloride exposure, self-cleaning properties, and anti-icing effectiveness. The results were promising, showcasing the coatings' potential for real-world implementations.

2. Materials and Methods

2.1. Material

SiO_2 particles, with diameters ranging from 1 to 10 μm , were procured from Yichang Huifu (Yichang, China). ZrO_2 nanoparticles, characterized by a diameter range of 20–50 nm, came from Macklin Reagents (Shanghai, China). The silane coupling agent KH-570 (γ -Methacryloxypropyltrimethoxysilane) was utilized from Macklin Reagents (Shanghai, China). The silicone-modified acrylic emulsion was produced by Anhui Tengtuo (Chizhou, China). AR-grade toluene was provided by Tianjin Fuyu Fine Chemicals (Tianjin, China). Both ethanol and hydrochloric acid (36~38%) of AR-grade were secured from Guoyao (Shanghai, China). Sodium hydroxide of AR grade was sourced from Macklin Reagents (Shanghai, China), while AR-grade sodium chloride was supplied by Xilong (Shantou, China). All experiments used self-prepared ultrapure deionized water.

2.2. Modification of ZrO_2 Nanoparticles

Modified ZrO_2 nanoparticles were hydrophobically enhanced using silane coupling agent KH-570. The modification process began with the ZrO_2 nanoparticles being laid out in a sterile Petri dish. These particles were then dried at 60 °C in an electric drum air oven for 6 h. Subsequently, 4 g of these ZrO_2 nanoparticles were combined with 30 mL of toluene. This mixture was stirred at room temperature for 20 min, followed by 20 min of ultrasonic agitation. Afterward, 20 mL of a 10% concentration of silane coupling agent KH-570 was added, and the entire blend underwent 10 min of ultrasonic dispersion. This dispersion was transferred to a 250 mL three-necked flask and was agitated at 80 °C for 30 min. Post cooling to room temperature, the mixture underwent centrifugation at 10,000 $\text{r}\cdot\text{min}^{-1}$ for 30 min. The resulting substance was filtered using a vacuum filtration method to obtain the modified ZrO_2 nanoparticles. These were then dried in a vacuum oven at 100 °C for 6 h.

2.3. Preparation of $\text{ZrO}_2/\text{SiO}_2/\text{Silicone-Modified Acrylic Emulsion Superhydrophobic Coating}$

Adopting a spray technique to fabricate superhydrophobic coatings. Initially, 0.1 mL of silicone-modified acrylic emulsion was dissolved in 1 mL of ethanol. Following this, 0.04 g of modified ZrO_2 nanoparticles and 0.06 g of SiO_2 particles were added to the solution. The mixture was magnetically stirred for 20 min at ambient temperature and then ultrasonically dispersed for an additional 5 min, producing ethanol dispersion with inorganic particles.

In the next phase, a superhydrophobic coating was created. This was achieved by spraying 2 mL of the silicone-modified acrylic emulsion evenly at 4 MPa onto a 2.5 × 7.5 cm slide and then spraying zirconia silica ethanol dispersion. Subsequently, the coated sample was cured at 100 °C for 20 min. The unattached particles on the coating's surface were removed by air flow and the obtained coating was named MZS-0.1. By using a similar procedure, MZS-0 and MZS-0.2 were prepared by using 0 and 0.2 mL silicone-modified acrylic emulsion, respectively. For comparison, MS-0.1 was also prepared without modified ZrO_2 nanoparticles. The entire process is illustrated in Figure 1. The surface of ZrO_2 inorganic particles features a Zr-O-H structure, which interacts with the Si-O-H structure of KH-570, leading to the formation of a modified ZrO_2 with a Zr-O-Si structure. Additionally, KH-570 possesses a carbon-carbon double bond. This double bond undergoes a reaction with the corresponding double bond in the silicone-modified acrylic emulsion, resulting in the creation of a novel covalent bond.

Due to the water-based nature of the emulsion, it vigorously repels hydrophobic particles, making wetting challenging. Additionally, the emulsion's adhesion capacity is inferior in comparison to potent adhesives like epoxy resin. In conclusion, the emulsion's modest hydrophobic nature makes it challenging to achieve super hydrophobicity using the first method (directly incorporating fillers into resin). Direct coatings prepared by the second method (adhesive + particle) demonstrated subpar wear resistance. During experimentation, a uniform silicone-modified acrylic emulsion (2 mL) was initially sprayed onto

the glass substrate, followed by applying an ethanol suspension of particles application, with particles constituting about 5% of the coating's mass fraction. Some silicone-modified acrylic emulsion was pre-introduced into the ethanol suspension, enhancing the inter-particle bonding strength. Ethanol's rapid evaporation during curing ensures the resin and particles intertwine. Adding a specific resin quantity to the particle suspension before curing accelerates this intermingling, enabling a cure at 100 °C for 20 min, forming a dispersed transition zone between the particles and the resin. The emergence of this zone ensures hydrophilic nanoparticles and hydrophobic silicone-modified acrylic emulsion interpenetrate and adhere securely to the glass substrate.

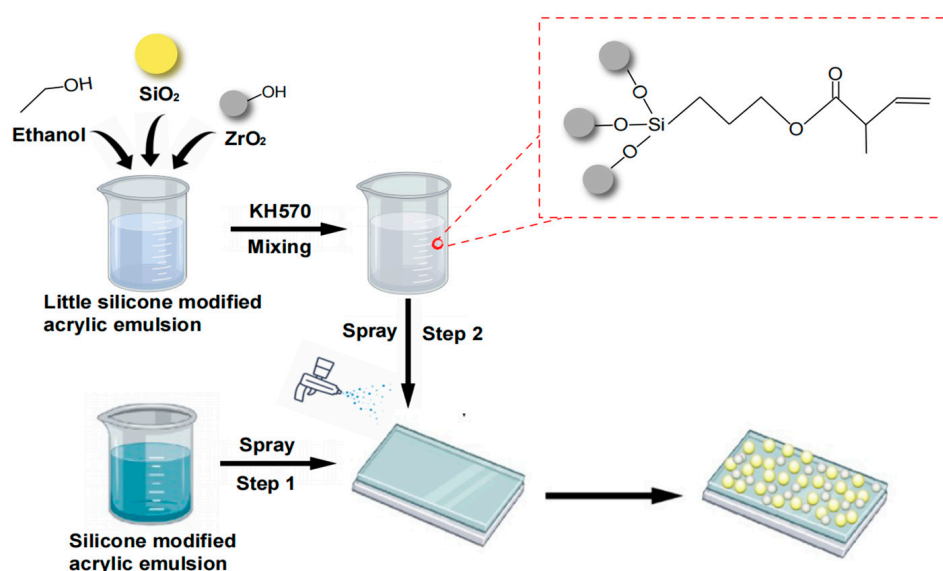


Figure 1. Schematic diagram of the preparation process of coating.

2.4. Chemical Structure Characterization

In this study, Nexus 670 FTIR instrument (Thermo Nicolet, MA, USA) was used to analyze the functional groups of ZrO_2 nanoparticles both before and after modification, and the KBr pressing technique was employed. The crystalline structures of the ZrO_2 nanoparticles, before and after modification, were assessed through X-ray diffraction (XRD) diagrams captured on the SmartLabTM X-ray diffractometer (Rigaku, Tokyo, Japan) set at 3 kW. Energy dispersive spectroscopy (EDS) was investigated using a JSM-6510 scanning electron microscopy (JEOL, Tokyo, Japan), which elucidated the elemental composition of the modified ZrO_2 nanoparticle surface. To probe the micro-nanometric structure of the $\text{ZrO}_2/\text{SiO}_2/\text{silane-acrylic acid}$ modified emulsion superhydrophobic coating, coat a layer of gold on the surface of the characterization sample and dry it in a vacuum. After the sample was prepared, SEM images were taken using a JSM-6510 scanning electron microscope (JEOL, Tokyo, Japan) with a 20 kV acceleration voltage. Additionally, the OLA4000 laser scanning confocal microscope (Olympus, Tokyo, Japan) provided three-dimensional visualizations of the diverse compositions present on the surface of the $\text{ZrO}_2/\text{SiO}_2/\text{silane-acrylic acid}$ modified emulsion superhydrophobic coating.

2.5. Measure the Contact and Rolling Angles

Contact angles and rolling angles were analyzed by using an SDC-350 contact angle measuring instrument (Dongguan Shengding Precision Instrument, Dongguan, China). the contact angles for all samples were measured at room temperature involved taking an average of five measurements with 6 μL water droplets dropping from 50 mm height. In the case of composite coatings with different compositions, the contact angle was measured directly on the surface using the same procedure. Additionally, the rolling angle for all composite coatings was determined using the same contact angle instrument. For this

measurement, samples were stabilized on the instrument platform. The rolling angle of 6 μL water droplets was ascertained by tilting the platform and altering its angle relative to the horizontal plane, until the droplets commenced sliding.

2.6. Wear Resistance

During the sandpaper abrasion test, a glass substrate coated with the $\text{ZrO}_2/\text{SiO}_2$ /silane-acrylic acid modified emulsion superhydrophobic layer underwent polishing using a 2000 # sandpaper. For each testing cycle, samples are pressed by a 200 g weight and slide 10 cm horizontally along the ruler. After a series of equidistant abrasion cycles, the contact and rolling angles of the coatings with different compositions were evaluated.

2.7. Chemical Stability

Researchers conducted two distinct immersion tests on superhydrophobic coatings with varying compositions. In the acid resistance test, we completely immersed nine samples of identical composition in hydrochloric acid ($\text{pH} = 1$, 0.1 mol/L). Every hour, we assessed the contact angle and rolling angle of one sample. Similarly, in the alkali resistance test, nine samples were fully immersed in a sodium hydroxide solution ($\text{pH} = 14$, 1 mol/L), with the contact angle and rolling angle of one sample evaluated hourly. For the salt tolerance test, seven samples were immersed in a 3.5% sodium chloride solution, and we measured the contact angle and rolling angle of one sample every 6 h.

2.8. Self-Cleaning Performance

Identical thicknesses of graphite powder and sand particles were sprinkled onto the surfaces of superhydrophobic coatings with varied compositions. To evaluate the self-cleaning capability, the coatings were tilted at a tilt angle of approximate 30°, and the ability of equal volume water droplets to roll off, collecting the contaminants, was observed. Additionally, the potential of these coatings to prevent stains was assessed by observing if a consistent volume of coffee solution left any residues when passed over them.

2.9. Anti-Icing Performance

50 μL water droplets were applied to a glass substrate coated with superhydrophobic materials of various compositions. This setup was placed inside a BL-LS400CDB refrigerator (Yeqi Electric Appliance, Shanghai, China). With a consistent cooling rate of 1 °C/min, cooling commenced from 0 °C. Throughout the process, a camera (image capture rate: 30 fps) was employed to capture the transition of water droplets to ice.

2.10. Water Droplet Bouncing, Water Flow Bending and Underwater Silver Light Reflection Performance

A water droplet of 6 μL volume and the water jet were observed to investigate the movement of it when touching the coating surface. Additionally, a unique silver reflection phenomenon associated with the superhydrophobic coating was noted. All fundamental images were captured by using an SDC-350 contact angle measuring instrument.

3. Results

3.1. Characterization of Modified ZrO_2 Nanoparticles

3.1.1. Microstructure

As shown in Figure 2, the pre-modified and modified ZrO_2 to XRD tests, and the observed peaks of the XRD pattern are indexed and compared with pure ZrO_2 (PDF#86-1450). It can be seen that the profile contains distinct characteristic peaks at 2 θ angles (24°, 28°, 31°, 34°, and 50°), which represent the optimal orientations of the five crystallographic planes (1 1 0), (−1 1 1), (1 1 1), (0 0 2), and (2 2 0), respectively. This XRD spectrum not only confirms the monoclinic crystal system of nano- ZrO_2 , but also indicates its own high crystallinity by its narrower linewidth [43]. More notably, the diffraction peaks before and

after the modification remain consistent, indicating that the structural integrity of the ZrO_2 nanoparticles is largely unaffected by the surface modification.

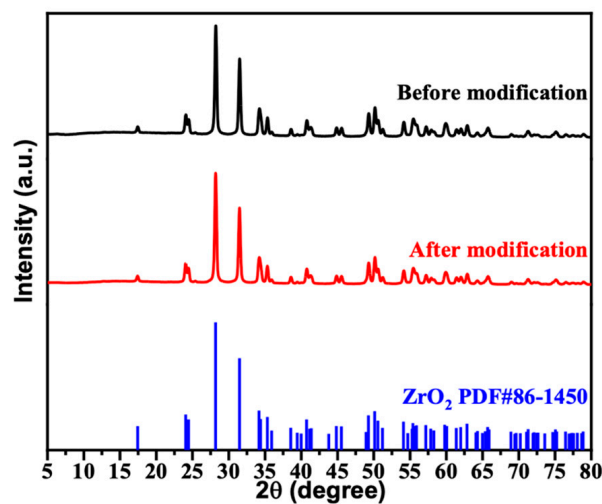


Figure 2. XRD diffraction pattern of zirconium dioxide.

Figure 3 presents the SEM image of the modified ZrO_2 , where the even dispersion of the Si element from the modifier KH-570 is evident. This uniform distribution confirms the successful modification of ZrO_2 . Furthermore, the coating surface displays a distinct rough and porous texture.

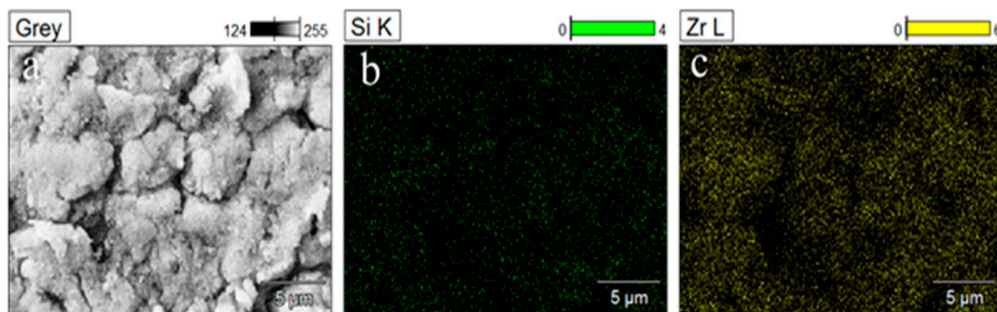


Figure 3. (a) SEM secondary electron image of modified zirconium dioxide, magnified 3000 times; (b) distribution of Si element in modified ZrO_2 nanoparticles; (c) distribution of Zr element in modified ZrO_2 nanoparticles.

3.1.2. Chemical Composition

Figure 4 presents the FTIR spectrum of ZrO_2 nanoparticles pre and post-modification. The modified ZrO_2 spectrum exhibits distinctive peaks: the one at 1107 cm^{-1} arises from the asymmetric stretching vibration of the -Si-O-C- group, the 1452 cm^{-1} peak represents the stretching vibration of the -COO- group, and the peak at 1635 cm^{-1} is associated with the C=C double bond stretching vibration. These peaks validate the dehydration reaction between hydrolyzed methacryloyloxypropyltrimethoxysilane molecules and ZrO_2 nanoparticles, corroborating the modification's success. This altered the original hydroxyl-rich, high-porosity coating to a surface with reduced energy, preventing pollutant infiltration and bolstering the coating's environmental stability [44].

3.2. Characterization of $\text{ZrO}_2/\text{SiO}_2/\text{Silicone}$ -Modified Acrylic Emulsion Superhydrophobic Coatings with Different Components

3.2.1. Micromorphology

Figures 5 and 6 display SEM images of three different coatings. Microscopic morphology of the MZS-0.1 coating surface is shown in Figure 5a–c. The modified ZrO_2 nanopar-

ticles cluster on the surface, creating large, distinctly aggregate spheres with substantial gaps between them. This micro-nano structure efficiently captures air while repelling water molecules, ensuring the coating's superhydrophobic nature. Figure 5d demonstrates that droplets cannot directly associate with the MZS-0.1 superhydrophobic coating and easily roll off its surface.

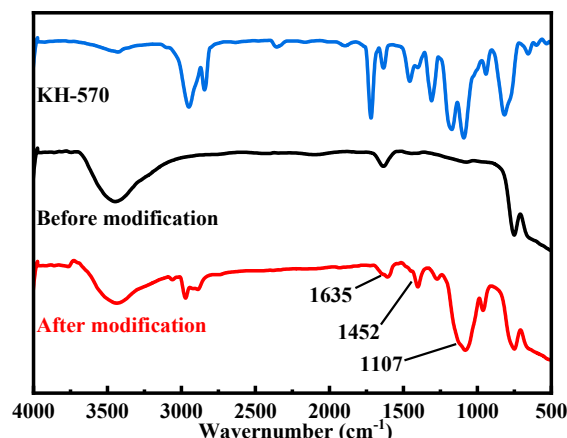


Figure 4. Infrared spectrum of ZrO_2 and KH-570.

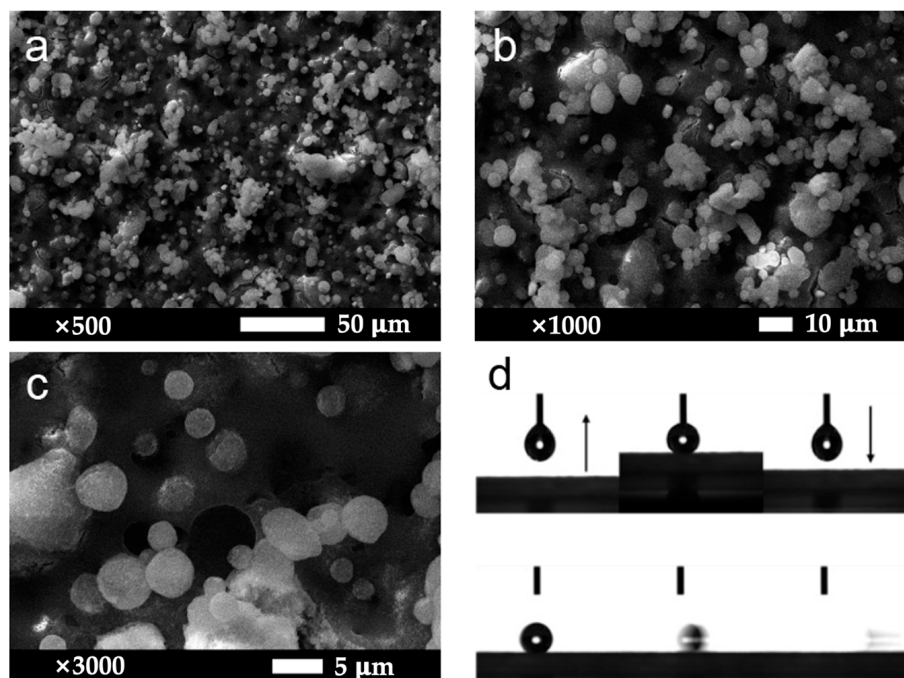


Figure 5. (a–c) Microscopic morphology images of the MZS-0.1 coating surface, magnified 500 times, 1000 times, and 3000 times in order; (d) the 8 μL droplet cannot be directly picked up with the MZS-0.1 superhydrophobic coating, and the droplet is very easy to roll on the MZS-0.1 coating.

Figure 6a,b illustrates the surface morphology of the MS-0.1 coating, revealing that it is less effective than the MZS-0.1 coating in creating air layer voids critical for superhydrophobicity. Larger particle sizes in MS-0.1 coating result in less surface voids, which adversely affect the nanostructure essential for optimal performance. To preserve the essential micro-nano structure in the superhydrophobic coating, it is necessary to mix modified ZrO_2 nanoparticles with SiO_2 . This blend may improve the distribution of initially clustered particles and encourage the formation of large clusters and voids. In contrast, as observed in Figure 6c,d, the pure silane-modified emulsion coating displays a smoother surface devoid of the aforementioned micro-nano structures.

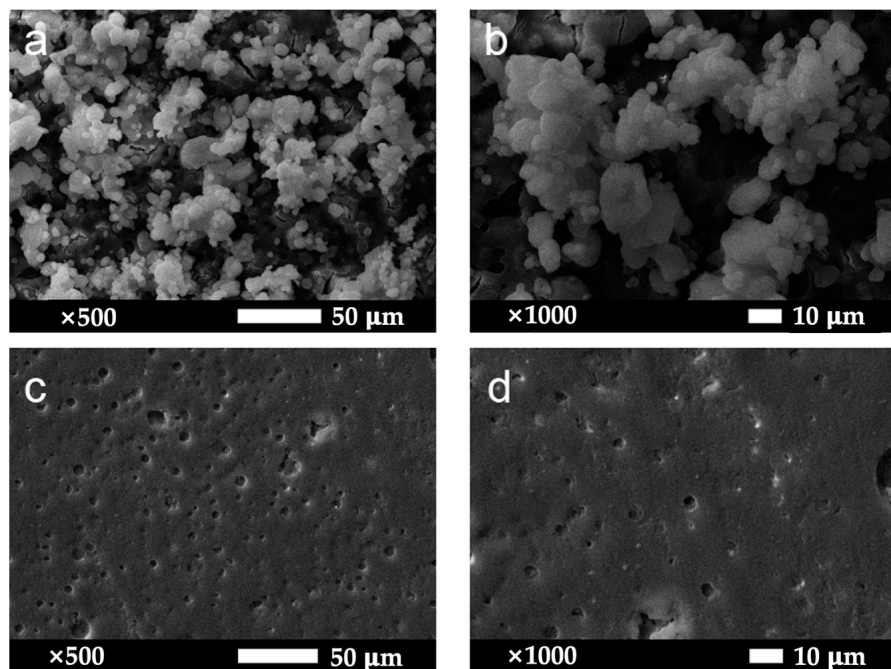


Figure 6. (a,b) Microscopic morphology images of the MS-0.1 coating surface, magnified 500 times, 1000 times in order; (c,d) images of the surface micromorphology of pure silicone-modified acrylic emulsion coating, magnified 500 times and 1000 times, respectively.

Figure 7 presents the CLSM images of various coatings, aligning with the SEM findings. The MZS-0.1 coating's surface (Figure 7e,f) displays pronounced orderly convex frame, especially when juxtaposed with the smoother surface of the pure silane-modified emulsion coating (Figure 7a,b). Compared with pure silicone-modified acrylic emulsion coating (height differential of less than 10 μm), the MZS-0.1 coating showed a height disparity reaching nearly 100 μm . Additionally, the MS-0.1 coating showed a height disparity reaching approximate 70 μm . This may be due to micro/nano hierarchical structure of $\text{SiO}_2/\text{ZrO}_2$. The surface of the MS-0.1 coating, as illustrated in Figure 7c,d, exhibits a less height differential than MZS-0.1 coating, which is not conducive to the formation of suitable sized voids for capturing air.

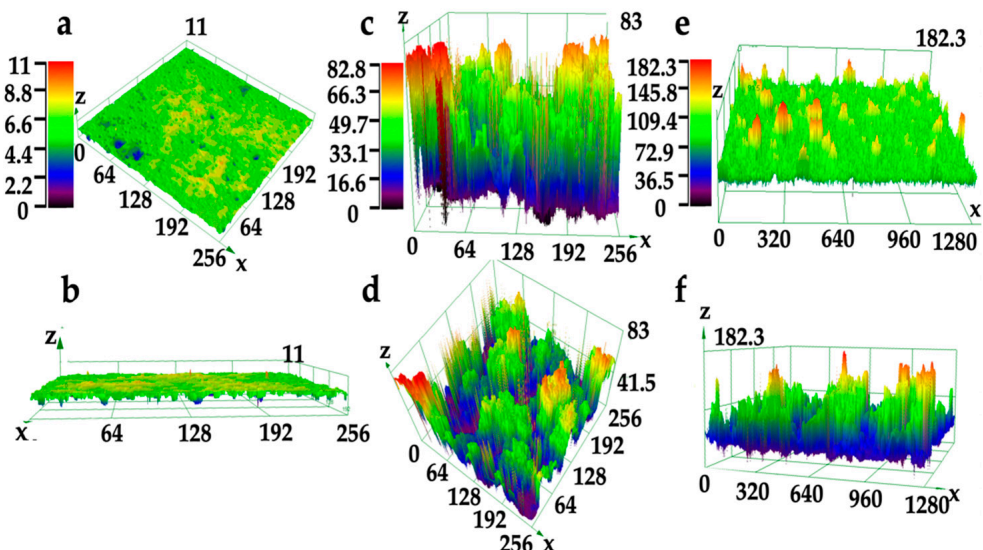


Figure 7. The CLSM images of various coatings: (a,b) pure silicone-modified acrylic emulsion coating surface; (c,d) MS-0.1 coating surface; (e,f) MZS-0.1 coating surface.

3.2.2. Hydrophobicity

Figure 8 presents the contact and rolling angles for four coatings: MZS-0, MZS-0.1, MZS-0.2, and MS-0.1. The data indicate that MZS-0 exhibits superhydrophobic properties, whereas the remaining coatings—MZS-0.1, MZS-0.2, and MS-0.1—display only partial hydrophobicity, as evidenced by their rolling angles ranging from 5 to 10 degrees.

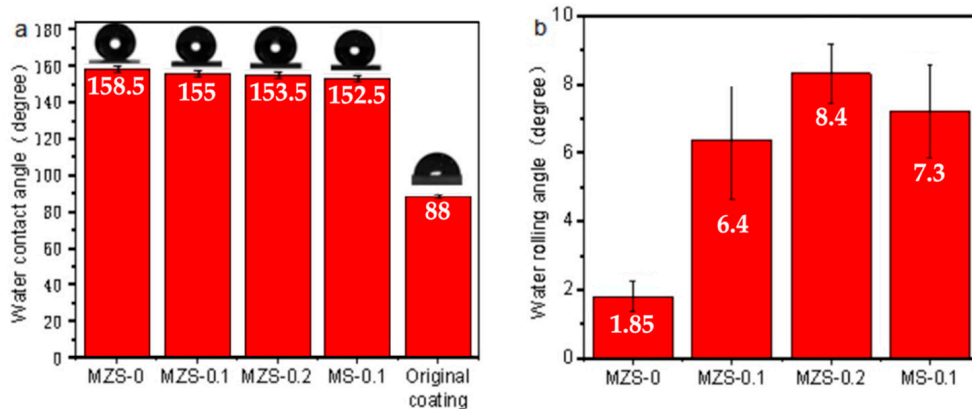


Figure 8. (a) Contact angle of different coatings; (b) rolling angle of different coatings.

As the silicone-modified acrylic emulsion content increases, the superhydrophobic coating's hydrophobic nature decreases, evident from the increasing roll-off angle. The contact angle of the pure silane-modified emulsion coating registers at 88° relative to the horizontal plane, lacking any superhydrophobic traits. It is evident that the silane-modified emulsion's over-wetting of hydrophobic particles results in a diminished contact angle and a heightened rolling angle. This phenomenon is attributed to the high surface free energy of the silicone-modified acrylic emulsion, which increases the superhydrophobic coating's high surface free energy. Concurrently, excessive silicone-modified acrylic emulsion infiltration into surface ZrO₂/SiO₂ nanoparticles causes underexposure of these nanoparticles, compromising the micro-nano surface structure and subsequently decreasing the superhydrophobic coating's surface roughness [45].

The comparison of coating contact angle and rolling angle is shown in Table 1 [46–50] where ZrO₂/SiO₂/silicone-modified acrylic emulsion coating has a significant hydrophobic effect.

Table 1. Comparisons of different coatings by contact angle and rolling angle tests.

Coating Composition	Preparation Process	Contact Angle (CA)	Rolling Angle (RA)	Ref.
316L/nano-TiO ₂ /TMPSi	one-step EPD	168°	3.1°	[46]
PS/OTS/SS	Sol-gel	157.5°	6°	[47]
MTES/SiO ₂ /MOH	Sol-gel	153°	9°	[48]
PDMS/MTCS/SiO ₂ /TiO ₂	Spray	151°	9°	[49]
F-PE/SiO ₂	Template	158°	4°	[50]
ZrO ₂ /SiO ₂ /siloxane-modified acrylic emulsion	Spray	158.5°	1.85°	This work

3.3. Wear Resistance of ZrO₂/SiO₂/Silicone–Acrylic Acid Modified Emulsion Superhydrophobic Coating

Figure 9 presents the contact and rolling angles of coatings with varying compositions after enduring consistent wear and tear. Given the same wear frequency, the MZS-0.1 coating's hydrophobicity declines after six wear cycles. In contrast, the MZS-0 coating with pure ZrO₂/SiO₂, without the addition of silicone-modified acrylic emulsion, maintains its rolling angle only once. After three successive wears, its contact angle drops below 150°, indicating a swift loss of super-hydrophobicity. This highlights the crucial role of silicone-modified

acrylic emulsion in bolstering the bond between the substrate and $\text{ZrO}_2/\text{SiO}_2$ surface nanoparticles, as well as the cohesion amongst the nanoparticles themselves. The contact angle trajectory for each coating remains predominantly stable, which can be ascribed to the transition region between the nanoparticle and silicone-modified acrylic emulsion layers arising from ethanol's evaporation. Within this zone, the sandpaper-induced texture post-rubbing closely mirrors its initial state, thus preserving super-hydrophobicity. Hence, integrating silicone-modified acrylic emulsion with nanoparticle ethanol dispersions can somewhat mitigate friction-induced hydrophobicity reduction. Yet, an excessive infusion of silicone-modified acrylic emulsion can escalate the particle dispersion's viscosity, complicating the spraying process and potentially leading to issues like cracking.

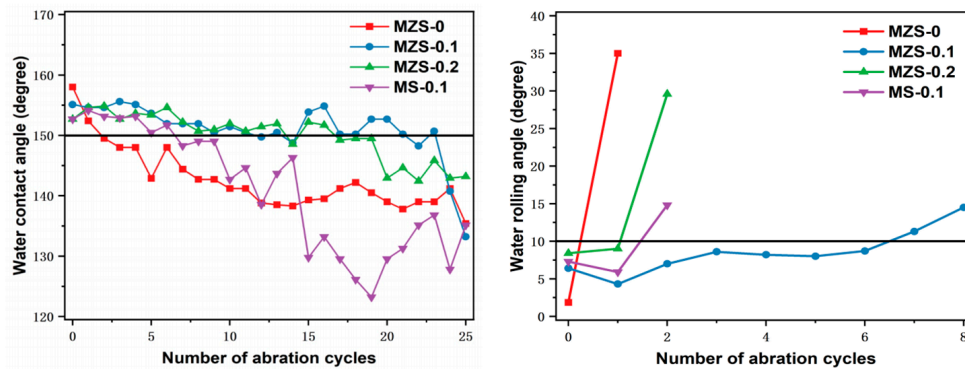


Figure 9. Wear resistance test of different organic hydrophobic coatings.

Upon incorporating the silicone-modified acrylic emulsion, the MS-0.1 coating loses its super-hydrophobicity post roughly one wear. However, the coatings embedded with ZrO_2 nanoparticles exhibited good wear resistance; notably, the MZS-0.1 coating maintained its super-hydrophobicity after six wear cycles. The superior hardness of ZrO_2 nanoparticles, compared to SiO_2 particles, suggests that ZrO_2 inclusion amplifies the superhydrophobic coating's resistance to wear.

3.4. Corrosion Resistance of $\text{ZrO}_2/\text{SiO}_2/\text{Silicone-Modified Acrylic Emulsion Superhydrophobic Coating}$

3.4.1. Acid and Alkali Corrosion Resistance

Figure 10 illustrates the changes in contact and rolling angles of the MZS-0.1 coating under exposure to a highly acidic environment with a pH value of 1. Notably, the MZS-0.1 coating's hydrophobicity declines within 1–2 h, as indicated by the increase in the rolling angle to above 5 degrees during this period. In comparison to the contact angle, the rolling angle is more susceptible to shifts in the surface's roughness and chemical composition of low-energy materials. Even trivial wear and corrosion can lead to pronounced discrepancies in the rolling angle. This heightened corrosion resistance in superhydrophobic coatings is attributed to the presence of a surface air layer, functioning as a shield against corrosive substances. This prevents these substances from infiltrating the coating, interacting with the inorganic nanoparticles, and damaging the surface's micro-nano structures. With the time passing, the superhydrophobic coating loses its unique properties.

On the other hand, as depicted in Figure 11, the MZS-0.1 coating does not demonstrate significant resistance to alkalinity in a potent alkaline environment with a pH of 14. The hydrophobic characteristics of the MZS-0.1 coating are entirely compromised within just an hour. The contact angle of the destroyed MZS-0.1 coating (63°) strays considerably from the 88° typical of pure silicone-modified acrylic emulsion coatings. This can be attributed to the potent alkali disrupting the chemical bonds between the surface's SiO_2 and ZrO_2 nanoparticles, which are interconnected by low surface energy organic polymers. This interference causes the initially hydrophobic particles to revert to a hydrophilic state, turning the hydrophobic coating more hydrophilic. Consequently, the water contact angle

for these hydrophilic particles is notably lower than that of the pure silicone-modified acrylic emulsion. After a 3 h immersion, the hydrophobic coating begins separating from its glass substrate. These observations suggest that alkali can destroy the interactions between hydrophobic coating and glass substrate.

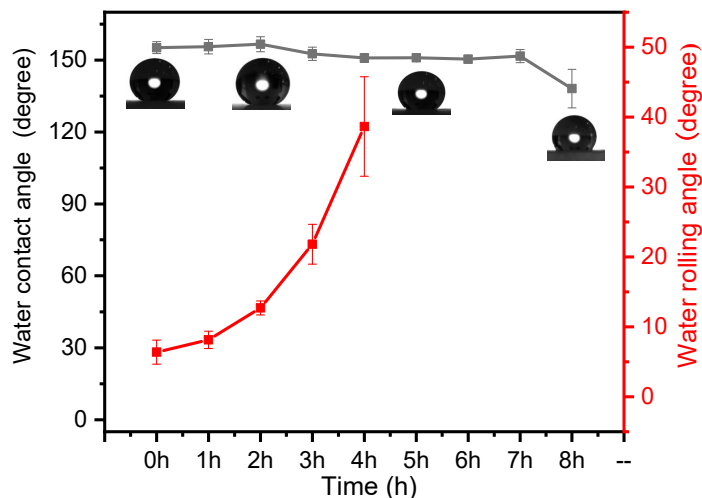


Figure 10. Changes in contact angle and rolling angle of MZS-0.1 coating in dilute hydrochloric acid solution with pH = 1.

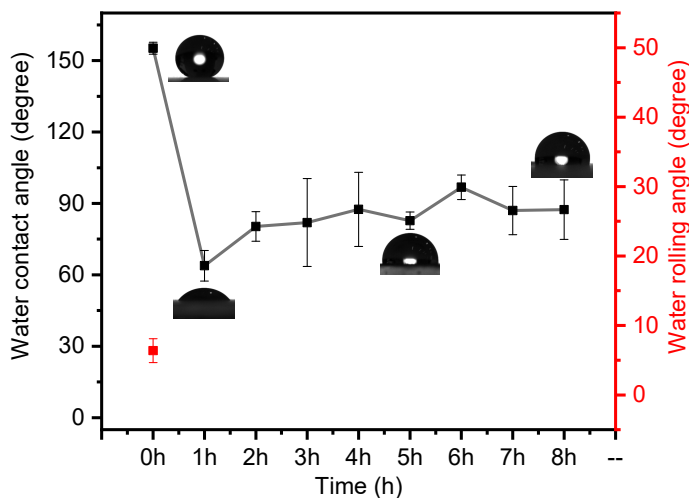


Figure 11. MZS-0.1 coating in sodium hydroxide solution with pH = 14.

3.4.2. Sodium Chloride Corrosion Resistance

Figure 12 presents the contact and rolling angles of the MZS-0.1 coating after varying durations of immersion in sodium chloride. The data illustrate that with an increase in immersion time, the MZS-0.1 coating's contact angle remains relatively stable at approximately 152°. However, it is observed that the rolling angle of the MZS-0.1 coating displayed significant variance with prolonged immersion, and its hydrophobicity descends after 6 h. This suggests minimal corrosion impact on the MZS-0.1 coating from the sodium chloride solution. In summary, the MZS-0.1 coating undeniably demonstrates superior resistance against sodium chloride corrosion.

3.5. Self-Cleaning Properties of ZrO₂/SiO₂/Silicone-Modified Acrylic Emulsion Superhydrophobic Coating

Figure 13 illustrates a images representation of graphite powder blanketing the surface of both the pure silicone-modified acrylic emulsion coating and the MZS-0.1 coating at a tilt angle of approximate 30°. Upon dropping the same quantity of distilled water droplets,

it is evident that the water beads clump together and find it challenging to roll off the pure silicone-modified acrylic emulsion coating. This behavior indicates a lack of self-cleaning attributes in the pure silicone-modified acrylic emulsion. Conversely, water droplets roll effortlessly on the MZS-0.1 coating, effectively shedding any attached dirt, highlighting the MZS-0.1 coating's superior self-cleaning capabilities.

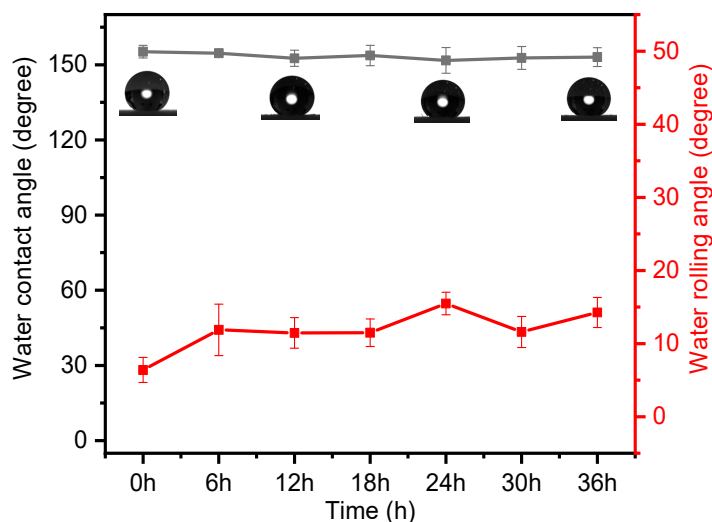


Figure 12. MZS-0.1 coating in 3.5% mass fraction sodium chloride solution.

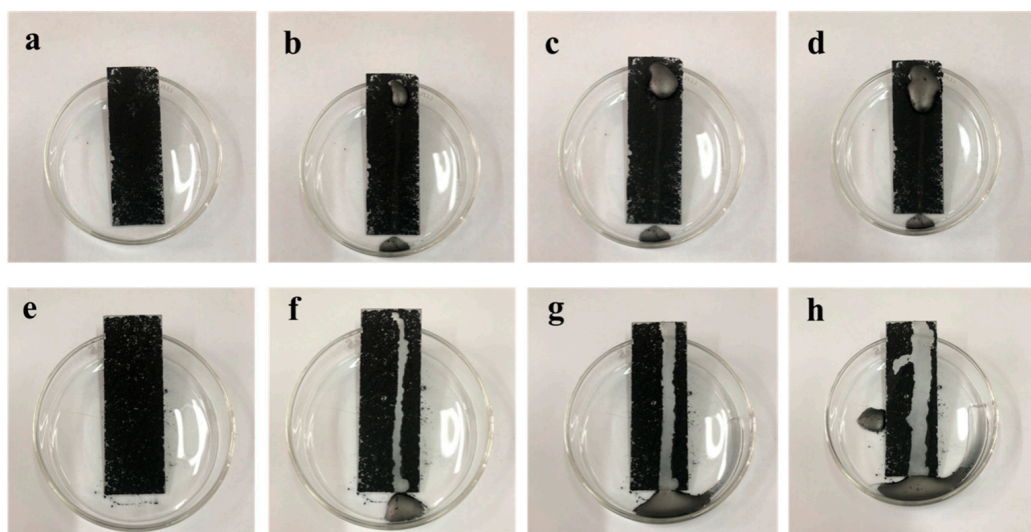


Figure 13. (a–d) Images of cleaning graphite powder on the surface of pure silicone–acrylic-modified emulsion coating; (e–h) images of graphite powder cleaning on MZS-0.1 coating surface.

Figure 14 depicts the cleaning process at a tilt angle of approximate 30° with identical distilled water droplet quantities on both the pure silicone-modified acrylic emulsion and MZS-0.1 coatings, both coated evenly with sand. The MZS-0.1 coating demonstrates a substantially more effective cleaning capacity than its pure silicone-modified acrylic emulsion counterpart, reiterating its excellent self-cleaning features.

In another test, shown in Figure 15, the same amount of sticky coffee liquid is poured at a tilt angle of approximate 30° onto both coatings. The MZS-0.1 coating impressively ensures that the coffee droplets glided off without leaving any residue, maintaining its uncontaminated state. On the other hand, evident marks are left behind by the coffee droplets on the pure silicone-modified acrylic emulsion coating, signifying some level of contamination.

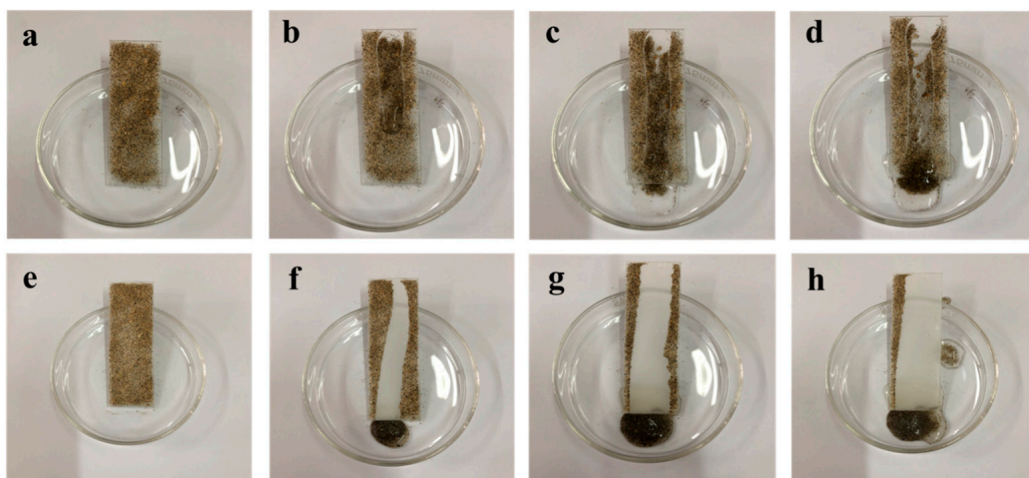


Figure 14. (a–d) Images of cleaning sand particles on the surface of pure silicone-modified acrylic emulsion coating; (e–h) images of cleaning sand particles on the surface of MZS-0.1 coating.

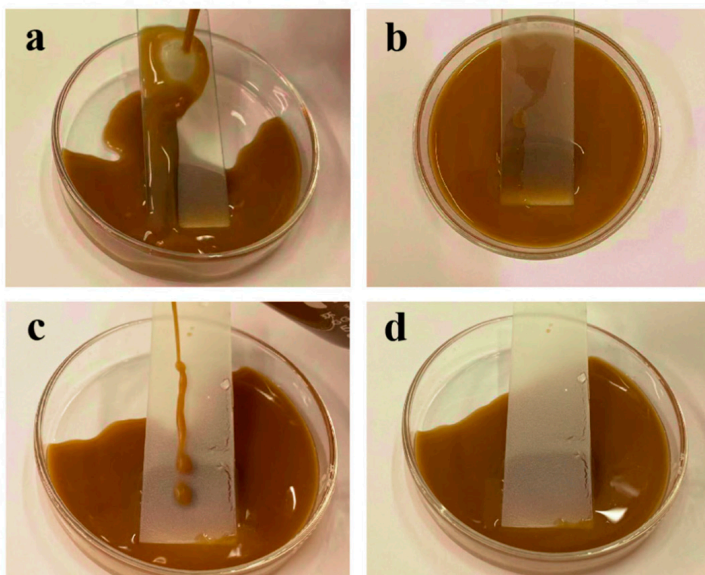


Figure 15. (a,b) Images of surface contamination of pure silicone-modified acrylic emulsion coating; (c,d) images of surface contamination of MZS-0.1 coating.

In light of the above observations, the coating has a good self-cleaning effect on solid particles such as graphite powder and fine sand particles and liquid pollutants such as coffee.

3.6. Anti-Icing Performance of ZrO_2/SiO_2 /Silicone-Modified Acrylic Emulsion Superhydrophobic Coating

Following the anti-icing evaluations on glass substrates, pure silicone-modified acrylic emulsion coatings, and MZS-0.1 coatings (as depicted in Figure 16), the initial time of ice formation serves as a pivotal metric in assessing the coatings' anti-icing capabilities. When cooled at a steady rate of $1\text{ }^{\circ}\text{C}/\text{min}$ starting from $0\text{ }^{\circ}\text{C}$, the crystallization time of water droplets on a glass substrate is approximately 4 min. In contrast, this time extends to 12 min for the pure silicone-modified emulsion coating—threefold longer than that of the glass—and to 17 min for the MZS-0.1 coating, which is over four times the duration of the glass substrate. All three samples reach a completely frozen state roughly eight minutes following the appearance of ice crystals.

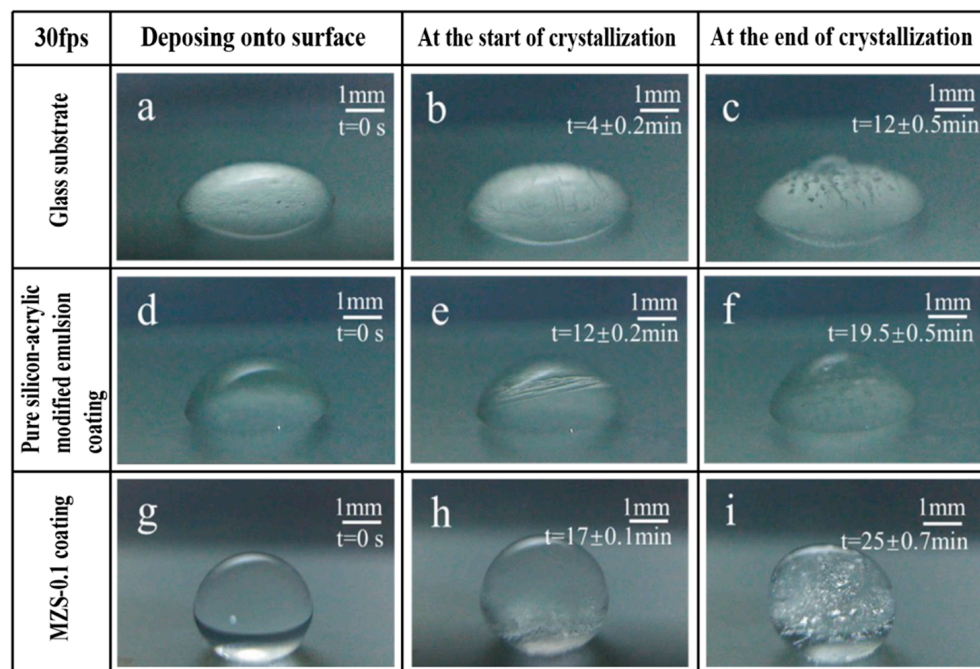


Figure 16. (a–c) Freezing process of a water droplet on glass substrate surfaces; (d–f) freezing process of a water droplet on pure silicon-acrylic modified emulsion coating surfaces; (g–i) freezing process of a water droplet on MZS-0.1 coating surfaces.

The smaller contact area between the spherical droplets and the coated surface leads to a reduced heat transfer rate and the presence of an air layer, which diminishes the direct contact between the water droplets and the superhydrophobic coating. This effectively decreases the likelihood of heterogeneous nucleation. Furthermore, crystallization kinetics principles suggest that the droplets on the superhydrophobic surface must overcome a significantly larger Gibbs free energy barrier to crystallize, particularly through heterogeneous nucleation. The magnitude of this barrier correlates with the increase in contact angle [51]. Consequently, the presence of modified ZrO₂ on the coating's surface substantially delays the crystallization time, suggesting that the coating possesses valuable anti-icing properties.

3.7. Water Droplet Bouncing, Water Flow Bending and Underwater Silver Light Reflection Properties of ZrO₂/SiO₂/Silicone-Modified Acrylic Emulsion Superhydrophobic Coating

A 6 μL water droplet exhibits pronounced elasticity when placed on the MZS-0.1 coating, as illustrated in Figure 17a–f, demonstrating a distinct bouncing effect [52]. When water is introduced to this coating using a syringe, it ricochets, similar to a laser beam reflecting off a mirror, as seen in Figure 17g. The air layer, residing on the surface, contributes to ricocheted behavior and enhances the elasticity observed in water droplets.

Figure 18 captures the underwater luminous reflection exhibited by the MZS-0.1 coating. When the superhydrophobic coating is submerged, the surface's air layer produces a lustrous, silver-like light, attributed to interface reflection. This interface reflection is intrinsically linked to the air layer on the surface.

In conclusion, the surface air layer is pivotal in enhancing the self-cleaning, corrosion resistance, drag minimization, and anti-icing attributes of superhydrophobic coatings. It supports several of the notable properties of these coatings [53]. A compromised surface air layer typically indicates that the superhydrophobic coating has been fully saturated, leading to the forfeiture of its superhydrophobic attributes [54].

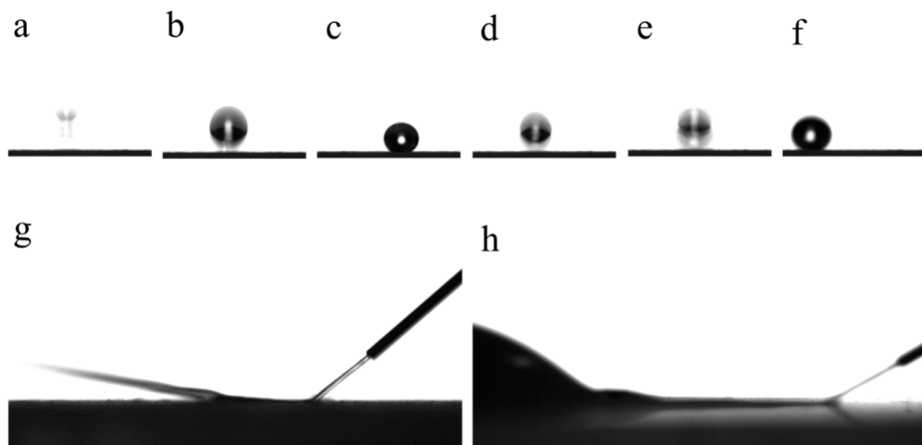


Figure 17. (a–f) Images of a 6 μL water droplet bouncing vertically on the MZS-0.1 coating from a height of 20 mm; (g) photo of water flow bending on the surface of MZS-0.1 coating; (h) photo of water flow accumulating on the surface of pure silicone-modified acrylic emulsion coating.

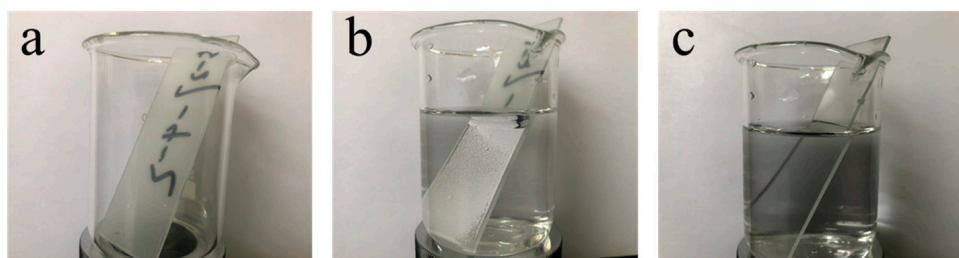


Figure 18. Photos of silver light reflection of superhydrophobic coating underwater; (a) MZS-0.1 coating in air; (b) MZS-0.1 coating in water; (c) pure silicone-modified acrylic emulsion coating in water.

4. Conclusions

In summary, we have successfully developed a method to fabricate four distinct coatings (MZS-0, MZS-0.1, MZS-0.2, MS-0.1) on glass substrates. This was achieved using a unique blend of γ -Methacryloyloxypropyltrimethoxysilane (KH570) modified $\text{ZrO}_2/\text{SiO}_2$ /silicone-modified acrylic emulsion to produce a superhydrophobic emulsion coating. One coating achieved super-hydrophobicity, registering a contact angle of 158.5 degrees and a rolling angle of 1.85 degrees. The inherent bonding strength of the silicone-modified acrylic emulsion ensures that these coatings can endure extensive mechanical wear, evident from their resistance to more than six abrasion cycles using 2000-grit sandpaper. Remarkably, the MZS-0.1 variant retains its superhydrophobic properties under extreme conditions, such as a 2 h immersion in strong acid ($\text{pH} = 1$, 0.1 mol/L) or a 6 h soak in salt water. Moreover, the MZS-0.1 coating showcases superior self-cleaning capabilities in an aerial environment. Due to the inclusion of KH570, the modified ZrO_2 surface significantly delays the crystallization of water droplets to 17 min, indicating a measure of anti-icing capability. This coating is also characterized by its surface elasticity and a distinctive underwater silvery sheen. The investigation into these coatings may reveal innovative approaches for developing effective superhydrophobic surfaces, specifically through the strategic use of emulsion mixtures with ZrO_2 and SiO_2 .

Author Contributions: Conceptualization, J.L.; Data curation, P.W. and Y.W.; Writing—original draft, J.B. and P.W.; Writing—review & editing, J.B. and Y.L. All authors have read and agreed to the published version of the manuscript.

Funding: This research received no external funding.

Institutional Review Board Statement: Not applicable.

Informed Consent Statement: Not applicable.

Data Availability Statement: Data are contained within the article.

Acknowledgments: The authors gratefully acknowledge the assistance from Gang Lu from NJTECH, and the staff from State Key Laboratory of Materials-Oriented Chemical Engineering.

Conflicts of Interest: The authors declare no conflict of interest.

References

- Marmur, A.; Della Volpe, C.; Siboni, S.; Amirkazli, A.; Drelich, J.W. Contact angles and wettability: Towards common and accurate terminology. *Surf. Innov.* **2017**, *5*, 3–8. [[CrossRef](#)]
- Abu-Thabit, N.Y.; Uwaezuoke, O.J.; Abu Elella, M.H. Superhydrophobic nanohybrid sponges for separation of oil/water mixtures. *Chemosphere* **2022**, *294*, 133644. [[CrossRef](#)]
- Sow, P.K.; Singhal, R.; Sahoo, P.; Radhakanth, S. Fabricating low-cost, robust superhydrophobic coatings with re-entrant topology for self-cleaning, corrosion inhibition, and oil-water separation. *J. Colloid. Interf. Sci.* **2021**, *600*, 358–372. [[CrossRef](#)] [[PubMed](#)]
- Lambley, H.; Schutzius, T.M.; Poulikakos, D. Superhydrophobic surfaces for extreme environmental conditions. *Proc. Natl. Acad. Sci. USA* **2020**, *117*, 27188–27194. [[CrossRef](#)]
- Maghsoudi, K.; Vazirinasab, E.; Momen, G.; Jafari, R. Icephobicity and durability assessment of superhydrophobic surfaces: The role of surface roughness and the ice adhesion measurement technique. *J. Mater. Proc. Technol.* **2021**, *288*, 116883. [[CrossRef](#)]
- Stamatopoulos, C.; Milionis, A.; Ackerl, N.; Donati, M.; de la Vallée, P.L.; von Rohr, P.R.; Poulikakos, D. Droplet Self-Propulsion on Superhydrophobic Microtracks. *ACS Nano* **2020**, *14*, 12895–12904. [[CrossRef](#)] [[PubMed](#)]
- Zhang, L.S.; Chen, K.S.; Yu, H.Z. Superhydrophobic Glass Microfiber Filter as Background-Free Substrate for Quantitative Fluorometric Assays. *ACS Appl. Mater. Interfaces* **2020**, *12*, 7665–7672. [[CrossRef](#)] [[PubMed](#)]
- Suryaprabha, T.; Ha, H.; Hwang, B.; Sethuraman, M.G. Self-cleaning, superhydrophobic, and antibacterial cotton fabrics with chitosan-based composite coatings. *Int. J. Biol. Macromol.* **2023**, *250*, 126217. [[CrossRef](#)] [[PubMed](#)]
- Isakov, K.; Kauppinen, C.; Franssila, S.; Lipsanen, H. Superhydrophobic Antireflection Coating on Glass Using Grass-like Alumina and Fluoropolymer. *ACS Appl. Mater. Interfaces* **2020**, *12*, 49957–49962. [[CrossRef](#)]
- Khaskhoussi, A.; Calabrese, L.; Proverbio, E. Anticorrosion Superhydrophobic Surfaces on AA6082 Aluminum Alloy by HF/HCl Texturing and Self-Assembling of Silane Monolayer. *Materials* **2022**, *15*, 8549. [[CrossRef](#)]
- Arablou, E.; Eshaghi, A.; Bakhshi, S.R. Investigation of chemical etching and surface modification effect on the superhydrophobic, self-cleaning and corrosion behaviour of aluminium substrate. *Bull. Mater. Sci.* **2022**, *45*, 176. [[CrossRef](#)]
- Doskocil, L.; Somanová, P.; Máslík, J.; Buchtík, M.; Hasonová, M.; Kalina, L.; Wasserbauer, J. Characterization of Prepared Superhydrophobic Surfaces on AZ31 and AZ91 Alloys Etched with ZnCl₂ and SnCl₂. *Coatings* **2022**, *12*, 1414. [[CrossRef](#)]
- Mani, K.A.; Belausov, E.; Zelinger, E.; Mechrez, G. Durable superhydrophobic coating with a self-replacing mechanism of surface roughness based on multiple Pickering emulsion templating. *Colloid Surf. A* **2022**, *652*, 129899. [[CrossRef](#)]
- Yanagishita, T.; Sou, T.; Masuda, H. Micro-nano hierarchical pillar array structures prepared on curved surfaces by nanoimprinting using flexible molds from anodic porous alumina and their application to superhydrophobic surfaces. *RSC Adv.* **2022**, *12*, 20340–20347. [[CrossRef](#)] [[PubMed](#)]
- Zhang, Y.; Zhu, X.R.; Liu, Y.J. Fabrication of durable superhydrophobic surface through silica-dissolution-assisted etching template approach. *Surf. Eng.* **2021**, *37*, 318–324. [[CrossRef](#)]
- Ghodrati, M.; Mousavi-Kamazani, M.; Bahrami, Z. Synthesis of superhydrophobic coatings based on silica nanostructure modified with organosilane compounds by sol-gel method for glass surfaces. *Sci. Rep.* **2023**, *13*, 548. [[CrossRef](#)]
- Hu, Y.H.; Ma, X.F.; Bi, H.H.; Sun, J.T. Robust superhydrophobic surfaces fabricated by self-growth of TiO₂ particles on cured silicone rubber. *Colloids Surf. A* **2020**, *603*, 125227. [[CrossRef](#)]
- Taurino, R.; Cannio, M.; Boccaccini, D.N.; Messori, M.; Bondioli, F. Preliminary study on the design of superhydrophobic surface by 3D inkjet printing of a sol-gel solution. *J. Sol-Gel Sci. Technol.* **2023**, *108*, 368–376. [[CrossRef](#)]
- Celik, N.; Torun, I.; Ruzi, M.; Esidir, A.; Onses, M.S. Fabrication of robust superhydrophobic surfaces by one-step spray coating: Evaporation driven self-assembly of wax and nanoparticles into hierarchical structures. *Chem. Eng. J.* **2020**, *396*, 125230. [[CrossRef](#)]
- Kim, H.; Nam, K.; Lee, D.Y. Fabrication of Robust Superhydrophobic Surfaces with Dual-Curing Siloxane Resin and Controlled Dispersion of Nanoparticles. *Polymers* **2020**, *12*, 1420. [[CrossRef](#)]
- Zhou, Y.C.; Liu, Y.; Du, F.L. Rational fabrication of fluorine-free, superhydrophobic, durable surface by one-step spray method. *Prog. Org. Coat.* **2023**, *174*, 107227. [[CrossRef](#)]
- Ghasemlou, M.; Le, P.H.; Daver, F.; Murdoch, B.J.; Ivanova, E.P.; Adhikari, B. Robust and Eco-Friendly Superhydrophobic Starch Nanohybrid Materials with Engineered Lotus Leaf Mimetic Multiscale Hierarchical Structures. *ACS Appl. Mater. Interfaces* **2021**, *13*, 36558–36573. [[CrossRef](#)] [[PubMed](#)]
- Sethi, S.K.; Kadian, S.; Gogoi, R.; Manik, G. Layer-by-layer fabrication of self-cleaning superhydrophobic surface made from Carboxymethylcellulose and ZnO quantum dots: A combined experimental and computational study. *Surf. Interfaces* **2023**, *37*, 102752. [[CrossRef](#)]

24. Zhou, Y.Q.; Liu, E.H.; Kang, J.H.; Zhao, S.; Wang, L.P.; Yan, H.Y.; Hu, C.X.; Han, J.H. A universal synthetic methodology of superhydrophobic protective film on various substrates with convenient and stable precursor. *Vacuum* **2023**, *210*, 111847. [\[CrossRef\]](#)
25. Ahmad, A.; Albargi, H.; Ali, M.; Batool, M.; Nazir, A.; Qadir, M.B.; Khalid, Z.; Arshad, S.N.; Jalalah, M.; Harraz, F.A. Differential carbonization-shrinkage induced hierarchically rough PAN/PDMS nanofiber composite membrane for robust multimodal superhydrophobic applications. *J. Sci. Adv. Mater. Devic.* **2023**, *8*, 100536. [\[CrossRef\]](#)
26. Juybari, H.F.; Karimi, M.; Srivastava, R.; Swaminathan, J.; Warsinger, D.M. Superhydrophobic composite asymmetric electrospun membrane for sustainable vacuum assisted air gap membrane distillation. *Desalination* **2023**, *553*, 116411. [\[CrossRef\]](#)
27. Kianfar, P.; Bongiovanni, R.; Ameduri, B.; Vitale, A. Electrospinning of Fluorinated Polymers: Current State of the Art on Processes and Applications. *Polym. Rev.* **2022**, *63*, 127–199. [\[CrossRef\]](#)
28. Lafraia, A.; Prieto, C.; Pardo-Figuerez, M.; Chiva, A.; Lagaron, J.M. Super-Repellent Paper Coated with Electrospun BioPolymers and Electrosprayed Silica of Interest in Food Packaging Applications. *Nanomaterials* **2021**, *11*, 3354. [\[CrossRef\]](#)
29. Qi, Y.L.; Yang, Z.B.; Huang, W.X.; Zhang, J. Robust superhydrophobic surface for anti-icing and cooling performance: Application of fluorine-modified TiO₂ and fumed SiO₂. *Appl. Surf. Sci.* **2021**, *538*, 148131. [\[CrossRef\]](#)
30. Ahmad, N.; Rasheed, S.; Ahmed, K.; Musharraf, S.G.; Najam-ul-Haq, M.; Hussain, D. Facile two-step functionalization of multifunctional superhydrophobic cotton fabric for UV-blocking, self cleaning, antibacterial, and oil-water separation. *Separ. Purif. Technol.* **2023**, *306*, 122626. [\[CrossRef\]](#)
31. Sumithraachchi, S.; Thilakarathna, B.; Bandara, J. TiO₂ encapsulated cross-linked polystyrene-polyacrylic acid membranes for waste oil-water separation. *J. Environ. Chem. Eng.* **2021**, *9*, 105394. [\[CrossRef\]](#)
32. Yap, S.W.; Johari, N.; Mazlan, S.A.; Ahmad, S.; Arifin, R.; Hassan, N.A.; Johari, M.A.F. Superhydrophobic zinc oxide/epoxy coating prepared by a one-step approach for corrosion protection of carbon steel. *J. Mater. Res. Technol.* **2023**, *25*, 5751–5766. [\[CrossRef\]](#)
33. Selvaraj, V.; Karthika, T.S.; Mansiya, C.; Alagar, M. ZnO nano grafted chitin-chitosan based hybrid composite coated super hydrophobic filter paper for water flow cleaning and oil-water separation applications. *New J. Chem.* **2023**, *47*, 13397–13408. [\[CrossRef\]](#)
34. Huang, J.D.; Li, M.M.; Ren, C.Y.; Huang, W.T.; Miao, Y.; Wu, Q.; Wang, S.Q. Construction of HLNPs/Fe₃O₄ based superhydrophobic coating with excellent abrasion resistance, UV resistance, flame retardation and oil absorbency. *J. Environ. Chem. Eng.* **2023**, *11*, 109046. [\[CrossRef\]](#)
35. Dong, H.Y.; Zhan, Y.Q.; Sun, A.; Chen, Y.W.; Chen, X.M. Magnetically responsive and durable super-hydrophobic melamine material. *Colloids Surf. A* **2023**, *662*, 130933. [\[CrossRef\]](#)
36. Hassan, N.; Fadhlani, M.M.; Al-Sulaimi, S.; Al-Buraihi, M.S.; Katubi, K.M.; Alrowaili, Z.A.; Khan, M.A.; Shoukat, R.; Ajmal, Z.; Abbas, F.; et al. Development of sustainable superhydrophobic coatings on aluminum substrate using magnesium nanoparticles for enhanced catalytic activity, self-cleaning, and corrosion resistance. *J. Mol. Liq.* **2023**, *383*, 122085. [\[CrossRef\]](#)
37. Ribeiro, A.C.; Soares, B.G.; Furtado, J.G.M.; Silva, A.A.; Couto, N. Superhydrophobic nanocomposite coatings based on different polysiloxane matrices designed for electrical insulators. *Prog. Org. Coat.* **2022**, *168*, 106867. [\[CrossRef\]](#)
38. Yang, J.L.; Chen, A.Y.; Liu, F.; Gu, L.J.; Xie, X.F.; Ding, Z.Y. Hybrid coating of polydimethylsiloxane with nano-ZrO₂ on magnesium alloy for superior corrosion resistance. *Ceram. Int.* **2022**, *48*, 35280–35289. [\[CrossRef\]](#)
39. Celik, N.; Sezen, B.; Sahin, F.; Ceylan, A.; Ruzi, M.; Onses, M.S. Mechanochemical Coupling of Alkylsilanes to Nanoparticles for Solvent-Free and Rapid Fabrication of Superhydrophobic Materials. *ACS Appl. Nano Mater.* **2023**, *6*, 14921–14930. [\[CrossRef\]](#)
40. Qi, Y.L.; Yang, Z.B.; Chen, T.T.; Xi, Y.L.; Zhang, J. Fabrication of superhydrophobic surface with desirable anti-icing performance based on micro/nano-structures and organosilane groups. *Appl. Surf. Sci.* **2020**, *501*, 144165. [\[CrossRef\]](#)
41. Zhou, L.; Zhao, X.Y.; Ju, G.N. Functionally Integrated Device with Robust and Durable Superhydrophobic Surface for Efficient, Continuous, and Recyclable Oil-Water Separation. *Adv. Mater. Interfaces* **2022**, *9*, 2101449. [\[CrossRef\]](#)
42. Yu, T.; Zhao, Y.P.; Zheng, P.; Wang, L.Y.; Yan, Z.H.; Ge, D.T.; Yang, L.L. Ultra-durable superhydrophobic surfaces from 3D self-similar network via co-spraying of polymer microspheres and nanoparticles. *Chem. Eng. J.* **2021**, *410*, 128314. [\[CrossRef\]](#)
43. Mallakpour, S.; Mani, L. The Special Modifiers Containing *N*-Trimellitylimido-L-Amino Acids for the Surface Modification of Nano ZrO₂. *Synth. React. Inorg. Met* **2016**, *46*, 394–399. [\[CrossRef\]](#)
44. Huang, J.C.; Liu, Y.; Cao, Y.Y.; Liu, Q.; Shen, J.; Wang, X.D. Durable silica antireflective coating prepared by combined treatment of ammonia and KH570 vapor. *J. Coat. Technol. Res.* **2019**, *16*, 615–622. [\[CrossRef\]](#)
45. Li, C.L.; Sun, Y.C.; Cheng, M.; Sun, S.Q.; Hu, S.Q. Fabrication and characterization of a TiO₂/polysiloxane resin composite coating with full-thickness super-hydrophobicity. *Chem. Eng. J.* **2018**, *333*, 361–369. [\[CrossRef\]](#)
46. Emarati, S.M.; Mozammel, M. Efficient one-step fabrication of superhydrophobic nano-TiO₂/TMPSi ceramic composite coating with enhanced corrosion resistance on 316L. *Ceram. Int.* **2020**, *46*, 1652–1661. [\[CrossRef\]](#)
47. Sutar, R.S.; Latthe, S.S.; Gcharge, N.B.; Gaikwad, P.P.; Jundle, A.R.; Ingole, S.S.; Ekunde, R.A.; Nagappan, S.; Park, K.H.; Bhosale, A.K.; et al. Facile approach to fabricate a high-performance superhydrophobic PS/OTS modified SS mesh for oil-water separation. *Colloids Surf. A Physicochem. Eng. Asp.* **2023**, *657*, 130561. [\[CrossRef\]](#)
48. Mahadik, S.A.; Mahadik, S.S. Surface morphological and topographical analysis of multifunctional superhydrophobic sol-gel coatings. *Ceram. Int.* **2021**, *47*, 29475–29482. [\[CrossRef\]](#)

49. Jumrus, N.; Suttanon, N.; Sroila, W.; Tippo, P.; Panthawan, A.; Thongpan, W.; Kumpika, T.; Sroila, W.; Rianyoi, R.; Singjai, P.; et al. Durability and photocatalytic activity of superhydrophobic gypsum boards coated with PDMS/MTCS-modified SiO₂-TiO₂ NPs. *Mater. Lett.* **2023**, *330*, 133342. [[CrossRef](#)]
50. Wu, T.; Xu, W.H.; Guo, K.; Xie, H.; Qu, J.P. Efficient fabrication of lightweight polyethylene foam with robust and durable superhydrophobicity for self-cleaning and anti-icing applications. *Chem. Eng. J.* **2021**, *407*, 127100. [[CrossRef](#)]
51. Li, W.; Zhan, Y.L.; Yu, S.R. Applications of superhydrophobic coatings in anti-icing: Theory, mechanisms, impact factors, challenges and perspectives. *Prog. Org. Coat.* **2021**, *152*, 106117. [[CrossRef](#)]
52. Li, A.L.; Wang, G.F.; Ma, Y.W.; Zhao, C.Y.; Zhang, F.Y.; He, Q.; Zhang, F.W. Study on preparation and properties of superhydrophobic surface of RTV silicone rubber. *J. Mater. Res. Technol.* **2021**, *11*, 135–143. [[CrossRef](#)]
53. Liu, M.L.; Luo, Y.F.; Jia, D.M. Robust and repairable bulk polymeric coatings with continuous superhydrophobicity for design control and underwater display. *Compos. Part B Eng.* **2020**, *186*, 107799. [[CrossRef](#)]
54. Wang, G.F.; Li, A.L.; Li, K.S.; Zhao, Y.H.; Ma, Y.W.; He, Q. A fluorine-free superhydrophobic silicone rubber surface has excellent self-cleaning and bouncing properties. *J. Colloid Interface Sci.* **2021**, *588*, 175–183. [[CrossRef](#)]

Disclaimer/Publisher's Note: The statements, opinions and data contained in all publications are solely those of the individual author(s) and contributor(s) and not of MDPI and/or the editor(s). MDPI and/or the editor(s) disclaim responsibility for any injury to people or property resulting from any ideas, methods, instructions or products referred to in the content.